International Journal of Engineering Science Invention (IJESI)
ISSN (Online): 2319-6734, ISSN (Print): 2319-6726
www.ijesi.org ||Volume 10 Issue 12 Series I || December 2021 || PP 07-17

Numerical Design of Electro-Hydraulic Servo System for a Ship Rudder using PID-FLQR Controller

Khaled Tchakala[1], Yao Jianjun[1*], Suubi Racheal[2]
[1] *College of Mechanical and Electrical Engineering, Harbin Engineering University, Harbin, 150001, China.*
[2] *Fundamental Science on Nuclear Safety and Simulation Technology Laboratory, Harbin Engineering University, Harbin, 150001, China.*
[*] *Corresponding author: Yao Jianjun*

ABSTRACT: *The electro-hydraulic steering gear control system is extensively used in versatile industrial applications such as machinery systems, industrial robots, copious actuators in aircraft, automotive industries, and so on. To boost the steering gear performance, the controller must detain good perturbation rejections and must be weighted with the uncertainties and possible malfunctions of the sensors. With the aims of designing a novel steering gear's controller that highly satisfy the above requirements, in this paper, a stochastic model for an electrohydraulic servo system (EHSS) composed of a double rod linear actuator and a balanced rudder located behind the propeller for ship steering was proposed. To set a closed-loop control on the steering gear system, two controllers' models such as autotuned Proportional-Integral-Derivative (PID) controller based on Ziegler-Nichols's method and Feedforward controller based on Linear Quadratic Regulator Optimal feedback (FLQR) were considered. To achieve the proposed design, a combination of both controllers (PID-FLQR) was developed and the numerical simulation was performed under Simulink tools. The controllers' performances were evaluated using process and measurement noise perturbations and heavy load disturbances to represent sailing in random waves. The results revealed that the novel proposed PID-FLQR controller performed the optimum load rejection capability, resulting in the improvement of the ship's request for a steering gear system.*
KEYWORDS -*EHSS, Electro-hydraulic Steering Gear System, FLQR, PID, Ship Rudder.*

Date of Submission: 17-11-2021 Date of Acceptance: 01-12-2021

I. INTRODUCTION

Rudders are the essential steering devices for most ships. The essential duty of rudders is to produce forces for course-keeping and maneuvering. They are also used for emergency braking and roll stabilization in exceptional cases. Furthermore, rudders have a significant impact on propeller thrust effectiveness and whole ship resistance as much as they are essential to navigation safety and freight efficiency [1]. The major concern related to ship steering gear control system is the problem of course-keeping when navigating under the effects of changes in ship draft depth. This variation is caused by loading and unloading processes, ocean environmental factors, such as wind, wave, current, and changes in effective rudder inflow speed because of ship's complicated motions which led to the variation of ship navigational speed since it is known that viscous hydrodynamic forces are relevant to ship speed [2]. Moreover, electro-hydraulic servo system (EHSS) for steering gear which performance must overwhelm the problem related to the navigation conditions also face nonlinearities problems in the expression of flow rate such as the presence of the square root of the pressure in the flow expression; the multiplication of the square root by the open section of the servo valve and the sign function inside the square root in the servo valve [3]**.** Consequently, the output from the position control system of the rudder is inaccurate. To overcome those problems, advanced control methods are implemented at the design stage, as well as onboard during ship operation.

The advent of an autopilot system in marine engineering reduces helmsman's workload. Trajectory tracking systems have been developed in several studies. it includes a gain scheduling Proportional-Integral-Derivative (PID) controller whose tuning gains have been adjusted by genetic algorithms (GS-PID-GA) for path tracking control of unmanned surface vessels (USVs) [4]. Withal, to overcome the difficulties of modifying PID parameters, genetic algorithms are employed [5]. Besides, a ship course online self-optimization PID controller based on the optimization characteristics of the Beetle Swarm Optimization algorithm (BSO-PID) was designed[6], the result benchmarks the controller as a better control effect on ship course and can be arbitrarily set with unknown PID parameters. Additionally, the development of heading control schemes for the yaw angle of a USV by using a Fuzzy controller with the modified Line of Sight (LOS) law compared to conventional LOS guidance was investigated [7]**.** The results confirm the effectiveness of the proposed LOS approach. Moreover,

the Nomoto first-order model of the Marine Class Vessel was used to design an adaptive autopilot using the Backstepping approach for the Marine Class Vessel [8]. However, the majority of these sophisticated control algorithms have the drawbacks of being complex, expensive, and need a significant amount of computing work. [9]. Therefore, the classic PID control model is still successfully applied in ship steering control systems owing to its simplicity and cheapness advantages.

Due to the disadvantages of traditional valve control in EHSS such as low energy efficiency, complex systems, and low reliability [10], some authors proposed direct-drive volume control (DDVC) electro-hydraulic servo system to design a ship steering control system. For example, the Direct Drive Electro-Hydraulic (DDEH) servo rotary vane steering was presented [11]. The simulation results showed that DDEH rotary vane steering Gear is a promising ship steering equipment that can match performance criteria. A direct drive volume control EHSS was designed and the result obtained by the steering gears closed-loop systems showed high efficiency and good dynamic performances [12]. Furthermore, a simulation of a direct drive volume control actuator (DDVCA) revealed that DDVCA has smooth operation, quick response, high control accuracy and may be used to replace typical servo valve electro-hydraulic actuators in low-frequency response applications [13]. Although several control models have been widely developed for the steering gear control system, the combination of both PID and FLQR models for high-performance control features still lacks and therefore needs to be further improved.

In this paper, a stochastic model for an EHSS composed of a double rod linear actuator and a balanced rudder located behind the propeller based on a mathematical model which considers the actual sailing conditions was applied [2]. A novel combination of the classical controller with optimal controller (PID-FLQR) was implemented to investigate the behavior of the steering machinery system. The controller is weighted with the uncertainties and possible faults of the sensors such as process and measurement noise perturbations and heavy load disturbances. A performance valuation was executed by integrating hydraulic parameter variations and disturbances. Finally, the results were discussed and agree well with those of the previous published reports.

II. MATERIALS AND METHODS

2.1 Problem reformulation

The electro-hydraulic steering gear system considered for this work as exposed in Fig.1 is composed of a pump feeding the system with oil stored in the tank, a relief valve, and an accumulator which are intended to keep the supply pressure Ps constant. The electrical control input acts on the electrohydraulic servo valve to move its spool. The spool motion controls the oil flow from the pump to the double rod hydraulic linear actuator. The rudder is driven by the actuator through the tiller arm which transforms the linear displacement of the actuator into an angular displacement of the rudder. The rudder position feedback is provided by fitting transducers.

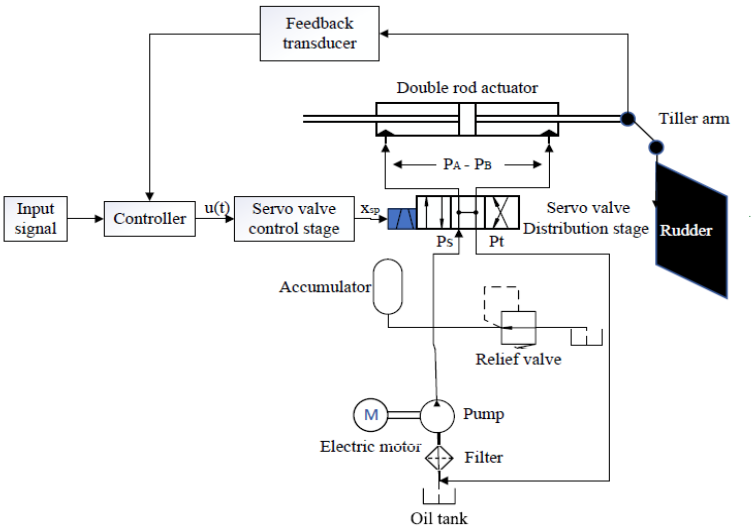

Figure 1. The scheme of the electro-hydraulic steering gear system of a ship, $u(t)$ is the control signal from the controller to the servo valve (V), p_A and p_B are the pressure inside the chambers A and B of the actuator (Pa), x_{sp} is the position of the spool (m), p_S is the supply pressure (Pa) and p_T is pressure to the tank (Pa).

Based on Fig.1, the closed-loop control system of the proposed EHSS for steering gear can be detailed as follow:

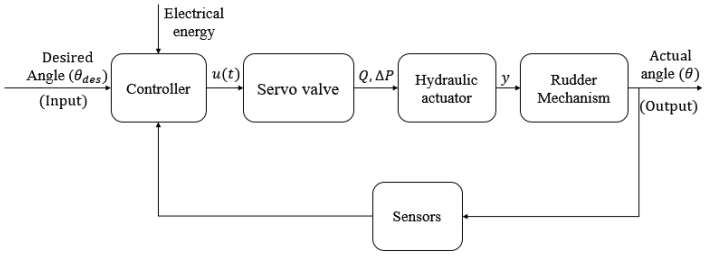

Figure 2. Block diagram describing the closed-loop control system of the EHSS for steering gear, Q and Δp are respectively the flow rate (m^3) and the difference of pressure (Pa) from the servo valve, y is the displacement of the hydraulic actuator's piston (m).

2.2 Modeling of ship steering gear system

The ship steering gear system consists of a driving system, and a steering system. It's a complex dynamic system running in an undefined environment because of large inertia, uncertainty, heavy load disturbance, and nonlinearities [14]. During loading and unloading processes, sea waves and wind actions in real conditions of sailing; changes occur in the draft depth and the motions of the ship. The parameters such as the navigational speed become uncertain and then are considered as uncertain disturbances. The steering gear drive shown in Fig.3 is composed of a two-stage EHSV, the first stage is called the control stage, and also termed as the proportion electromagnet receives the command as an electrical input. When the coils of the control stage are subjected to the electric control current, the magnetic field produces the spool's displacement in the distribution stage which is also called the pilot valve of the EHSV. The spool's displacement in the distribution stage produces a flow rate or difference of pressure in the double rod linear actuator which causes the linear displacement of the piston of the actuator. The linear displacement of the actuator's piston is then transformed into an angular displacement by the rudder mechanism.

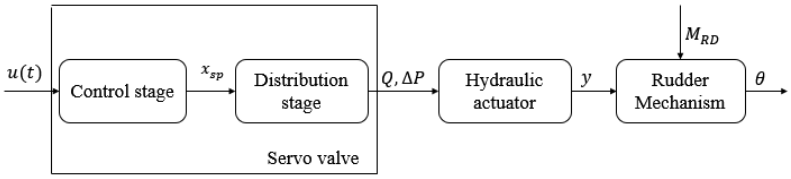

Figure 3. Block diagram illustrating the dynamics of the steering gear drive system, x_{sp} is the position of the spool (m), Q and Δp are respectively the flow rate (m^3) and the difference of pressure (Pa) from the servovalve, y is the displacement of the hydraulic actuator's piston (m), θ is the rudder's angular position.

2.2.1 Control stage of servo valve

An EHSV is a tool of proportional control of a hydraulic flow and/or pressure by an electrical control signal [15]. Referring to the relationship between the position of the servo-valve distribution spool and the control input signal established from a simplified model by [16],[17] and [18], the transfer function between the spool position and the control current is given by:

$$\frac{X_{sp}(s)}{I(s)} = \frac{k_{sp}}{\tau s + 1} \tag{1}$$

Where τ is the time constant (s), k_{sp} is the static gain of the servo valve (m / A).

2.2.2 Distribution stage of servo-valve

Distribution valves are classified according to the number of orifices through which the fluid can enter and exit, the number of spools, and the type of center when the valve is centered on the orifice. Some characteristics of valves are directly related to the geometry of their center. Thus, the type of center is a very important characteristic, because it determines the flow gain, i.e., the gain between the flow of the valve Q_L and the displacement of the distribution spool x_{sp} [19]. A 4-way critical center (zero overlaps) servo-valve is

therefore preferred to have a linear behavior. Considering $x_{sp} \geq 0$, the density and volume are constant, the flow equations at ports *A* and *B* are given by:

$$Q_A = C_D.w.x_{sp}.\sqrt{\frac{2}{\rho}(p_S - p_A)} \qquad Q_B = C_D.w.x_{sp}.\sqrt{\frac{2}{\rho}(p_B - p_T)} \tag{2}$$

2.2.3 Double-rod linear actuator

When the servo-valve distribution spool opens in the positive direction, the linear actuator moves under the action of the flow of the hydraulic fluid under pressure. A flow Q_A to the linear actuator creates an increase of pressure in chamber *A* of the linear actuator, and a flow Q_B leaving creates a decrease of pressure in chamber *B*. The pressure differential between the two chambers then creates a positive displacement *y* of the cylinder's rod.

In addition, the external loads applied to the linear actuator greatly vary the pressure inside the chambers, in turn influencing the flow through the servo-valve. This phenomenon will now be described using the equation of the rate of increase of pressure within a variable volume.

The pressure variations in chambers *A* and *B* gives:

$$\frac{\partial p_A}{\partial t} = \frac{\beta}{V_O + A.y}.\left(Q_A - C_{fint}(p_A - p_B) - C_{fext}.p_A - \frac{A}{\eta_{a_v}}.\frac{dy}{dt}\right)$$

$$\frac{\partial p_B}{\partial t} = \frac{\beta}{V_O - A.y}.\left(-Q_B + C_{fint}(p_A - p_B) - C_{fext}.p_B + \frac{A}{\eta_{a_v}}.\frac{dy}{dt}\right) \tag{3}$$

Where β is the compressibility modulus or Bulk modulus; η_{a_v} is the volumetric efficiency of the actuator; C_{fint} and C_{fext} ($s.m^4 / Kg$) are the internal and external leakage coefficients respectively between the two chambers; $\frac{\partial p_A}{\partial t}$ and $\frac{\partial p_B}{\partial t}$ are the variations of pressure in chambers *A* and *B*.

To analyze the fluid pressures on sides *A* and *B* of the actuator we assume that the transmission lines between the valve and the actuator are very short (small volumes of fluid exist on either side of the actuator), additionally, the load dynamics occur over a range of seconds and the pressure dynamics typically occur over a range of milliseconds, then it is usually safe to neglect the time variation of the pressure in favor of the time variation of the overall system, so the pressure transients that result from fluid compressibility are negligible. Using these assumptions, we can use the volumetric efficiency results to describe the volumetric flow rates in and out of the actuator:

$$Q_A = \frac{A}{\eta_{a_v}}.\frac{dy}{dt} \qquad Q_B = \frac{A}{\eta_{a_v}}.\frac{dy}{dt} \tag{4}$$

By introducing equation (4) in (3), we can determine the expressions of the pressures p_A and p_B:

$$p_A = -\frac{K_q^a}{K_c^a}.x_{sp} + \frac{A}{\eta_{a_v}K_c^a}.\frac{dy}{dt} \qquad p_B = -\frac{K_q^b}{K_c^b}.x_{sp} + \frac{A}{\eta_{a_v}K_c^b}.\frac{dy}{dt} \tag{5}$$

The actuator is double rod linear and will transform the hydraulic power into mechanical power to direct the rudder. Newton's second law will now be used to relate the external charge to the pressure in the chambers:

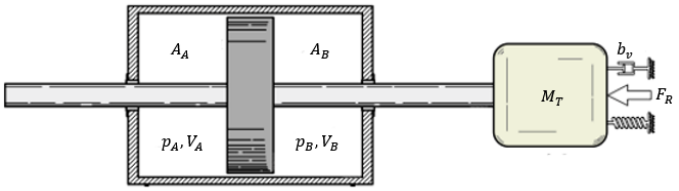

Figure 4. Description of the dynamics of the double linear actuator under internal and external forces: A_A, p_A and V_A are respectively the area (m^2), the pressure (Pa) and the volume of the liquid (m^3) in the chamber A. Similarly for chamber B, b_v is the internal friction coefficient, M_T is the total mass of the rudder mechanism, F_R represents the external forces applied on the actuator(N).

$$\eta_{af}.A\left(-\frac{K_q^a}{K_c^a}+\frac{K_q^b}{K_c^b}\right).X_{sp}-F_R=M_T.\frac{d^2y}{dt^2}+\left(b_v-\frac{\eta_{af}}{\eta_{a_v}}\left(\frac{A^2}{K_c^a}-\frac{A^2}{K_c^b}\right)\right).\frac{dy}{dt}+K_r.y \tag{6}$$

F_R represents the forces acting on the rudder, A is the surface on each other of the actuator, η_{af} is the force efficiency of the actuator, K_r is the stiffness of the load spring.

2.2.4 Hydrodynamic forces of the rudder

As illustrated in Fig.5, the linear displacement of the actuator's piton is transformed into an angular displacement by the rudder mechanism composed by a tiller arm, the rudder trunk and the rudder blade.

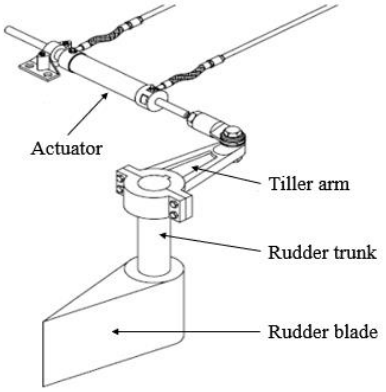

Figure 5. Description of motion transfer from the hydraulic actuator to the rudder through the tiller arm.

To avoid a rudder fold-over which consists of over-stress the components of the steering system, an offset angle (α)that relates to the ram to tiller geometry has been incorporated. This will allow enough mechanical leverage to have a completely "safe" setup (Fig.6).

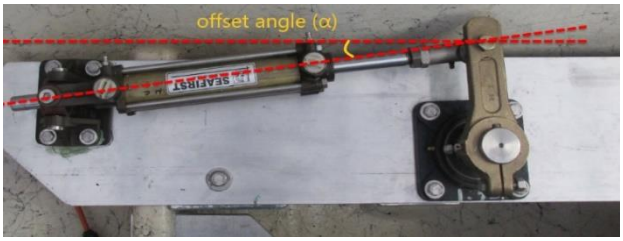

Figure 6. Actuator and tiller arm arrangement to avoid rudder fold-over.

Since the control angles are between: 0≤θ≤35°, it is assumed that:

$$y=l.\sin(\theta)\approx l.\theta \quad \rightarrow \quad Y(s)=l.\theta(s) \tag{7}$$

Applying Newton's law, we can deduce the relationship in Laplace domain between the voltage control input $U(s)$ and the desired angle $\theta(s)$:

$$\frac{\theta(s)}{U(s)} = \frac{K.k_{sp}.Z}{a\tau s^3 + (b\tau + a)s^2 + (c\tau + b)s + c} \tag{8}$$

Where Z is the voltage gain (A/V)

With: $K = \eta_{af} A\left(-\frac{K_q^a}{K_c^a} + \frac{K_q^b}{K_c^b}\right)$; $a = M_T l$; $b = \left(b_v - \frac{\eta_{af}}{\eta_{a_v}}\left(\frac{A^2}{K_c^a} - \frac{A^2}{K_c^b}\right)\right).l$; $c = K_r l + 1.2 \times \frac{F_N d}{l\cos(\alpha)}$

2.3 Controller implementation of Stochastic model and undefined disturbances

A general state-space mathematical description is given considering the dynamical system and uncertain and random disturbances:

$$\begin{cases} \dot{x}(t) = Ax(t) + Bu(t) + B_w w(t) \\ y(t) = Cx(t) + v(t) \end{cases} \tag{9}$$

Where, $x(t)$ is states vectors; $u(t)$ is input vector; $y(t)$ is output vector; $w(t)$ is random process noise disturbance; $v(t)$ is measurement noise; A is system matrix; B is input matrix; C is output matrix, B_w is process noise disturbance matrix which is equal to B.

$$A = \begin{bmatrix} -\frac{b\tau + a}{a\tau} & -\frac{c\tau + b}{a\tau} & -\frac{c}{a\tau} \\ 1 & 0 & 0 \\ 0 & 1 & 0 \end{bmatrix}; \; B = \begin{bmatrix} 1 \\ 0 \\ 0 \end{bmatrix}; \; C = \begin{bmatrix} 0 \\ 0 \\ \frac{K.k_{sp}.Z}{a\tau} \end{bmatrix}^T \tag{10}$$

2.3.1 Ziegler-Nichols autotuning PID

The objective of this section is to develop a PID controller based on the linearized state model of EHSS. The control signal is determined by:

$$u(t) = -\left[k_p e(t) + k_i \int e(t)\,dt + k_d \dot{e}(t)\right] \tag{11}$$

Where k_P, k_i, k_d represent the different controller gains and $e(t) = y(t) - y_{des}(t)$ is the error between the input and of the output of the signal. The values of the PID controller gains are shown in Table 1.

Table 1. Ziegler-Nichols PID gains values

Gains	k_p	k_i	k_d
Values	$0.6 \times k_u$	$\frac{P_u}{2}$	$\frac{P_u}{8}$

The value of the critical gain (k_u) and that of the critical period (P_u) can be determined experimentally or analytically. To obtain a literal value of these gains according to the parameters of the EHSS, we use the analytical method by considering the equation (8). The control law of the PID controller is then given by:

$$u(t) = -\left[-0.6\frac{(b\tau + a)(c\tau + b) - a\tau c}{a.\tau.K.k_{sp}.Z}e(t) + \pi\sqrt{\frac{a\tau}{c\tau + b}}\int e(t)\,dt + \frac{\pi}{4}\sqrt{\frac{a\tau}{c\tau + b}}\dot{e}(t)\right] \tag{12}$$

2.3.2 Feedforward based on Linear Quadratic Regulator

To obtain optimal performance of the system (9) through LQR formulation, the following quadratic cost function should be minimized.

$$J = \frac{1}{2}\int_0^\infty \left[x^T(t)Qx(t) + u^T(t)Ru(t)\right]dt \tag{13}$$

Where $Q = Q^T \geq 0, \quad R = R^T > 0$ are weighting matrices. In general, the weighting matrix Q is varied, keeping R fixed, to obtain optimal control signal from the linear quadratic regulator.

The minimization of the above cost function gives the optimal control input as:

$$u(t) = -Kx(t) \tag{14}$$

Where $K = R^{-1}B^T P$ is the LQR optimal feedback gain of our system and P is the solution of the algebraic Riccati Equation:

$$A^T P(t) + P(t)A + Q - P(t)BR^{-1}B^T P(t) = 0 \tag{15}$$

An optimal feedforward gain N is then added to produce zero steady-state error at the output in absence of modeling errors.

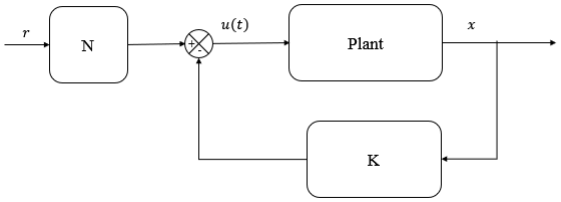

Figure 7. A block diagram describing FLQR closed-loop: r is the reference input(desired angle), $u(t)$ is the control law , K is the optimal feedback gain, N is the feedforward gain and x are the states variables.

The closed-loop of the FLQR controller is described in Fig.7, the feedforward gain N amplifies the reference input signal r to produce zero steady-state error at the output. The states variables x are measured and amplified with the optimal feedback gain K , the control law is therefore given by:

$$u(t) = Nr - Kx(t) \tag{16}$$

The closed-loop system model becomes:

$$\begin{cases} \dot{x}(t) = (A - BK)x(t) + BNr + B_w w(t) \\ y(t) = Cx(t) + v(t) \end{cases} \tag{17}$$

The expression of the feedforward gain is given by:

$$N = -\frac{1}{C(A - BK)^{-1}B} \tag{18}$$

The control law of the FLQR controller for the electro-hydraulic steering gear is given by:

$$u(t) = -\left[\frac{1}{C(A - BK)^{-1}B}\right] r - \left[R^{-1}B^T P\right] x(t) \tag{19}$$

2.3.3 PID-Feedforward control based on Linear Quadratic Regulator

By combining the equations (12) and (19), the reference input in the equation (19) is then replaced by the control law of the PID controller in the equation (12). The PID-FLQR control law of the electro-hydraulic steering gear is given by:

$$u(t) = \frac{1}{C(A - BK)^{-1}B}\left[-0.6\frac{(b\tau + a)(c\tau + b) - a\tau c}{a.\tau.K.k_{sp}.Z}e(t) + \pi\sqrt{\frac{a\tau}{c\tau + b}}\int e(t)\,dt + \frac{\pi}{4}\sqrt{\frac{a\tau}{c\tau + b}}\dot{e}(t)\right] - \left[R^{-1}B^T P\right]x(t) \tag{20}$$

Fig.8 shows the Simulink diagram of the combination of PID-FLQR controller for ship steering gear system:

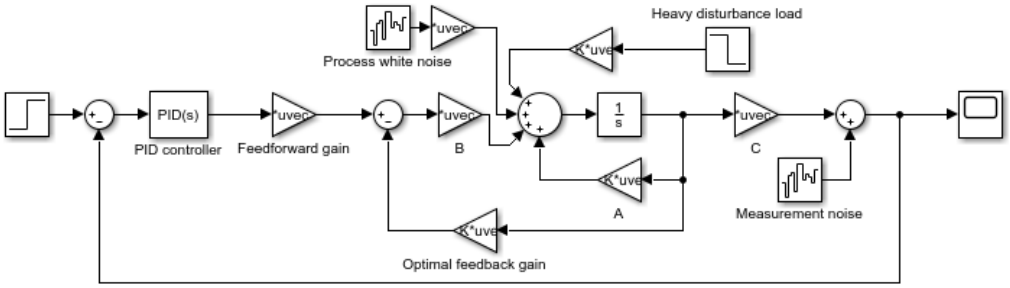

Figure 8. The block diagram of the PID-FLQR controller, A is the system matrix, B is the input matrix and C is the output matrix.

III. SIMULATION RESULTS

The steering gear drive system parameters and reduced ship model parameters are put into the transfer function of the control signal u and the rudder angle θ . these parameters are used for carrying out the simulations as indicated in Table 2 below.

Table 2. Ship, rudder and EHSV basics parameters

Parameters	Values
length of ship (between perpendiculars) (m)	3.763
Height of rudder (m)	0.162
Breadth of rudder (m)	0.1
Mass density of water (kg/m^3)	1032
Fluid bulk modulus (N/m^2)	7×10^8
Fluid mass density (kg/m^3)	875
Leakage coefficient (N.s)	10^{-12}
Supply pressure (Pa)	17×10^6
Viscous damping coefficient (N.m.s)	0.01
Rudder total torque (N.m)	185.329
Heavy load disturbance torque (N.m)	278
Ship speed (m/s)	10

These parameters are useful for establishing the model of the steering gear system of the ship. By implementing them, we can simulate and observe the open-loop response of the steering gear system. Then, a controller can be implemented to the system for a better response as desired. The open-loop response curve shows that the ship steering system is non-self-balanced and can be observed in Fig.9(a).

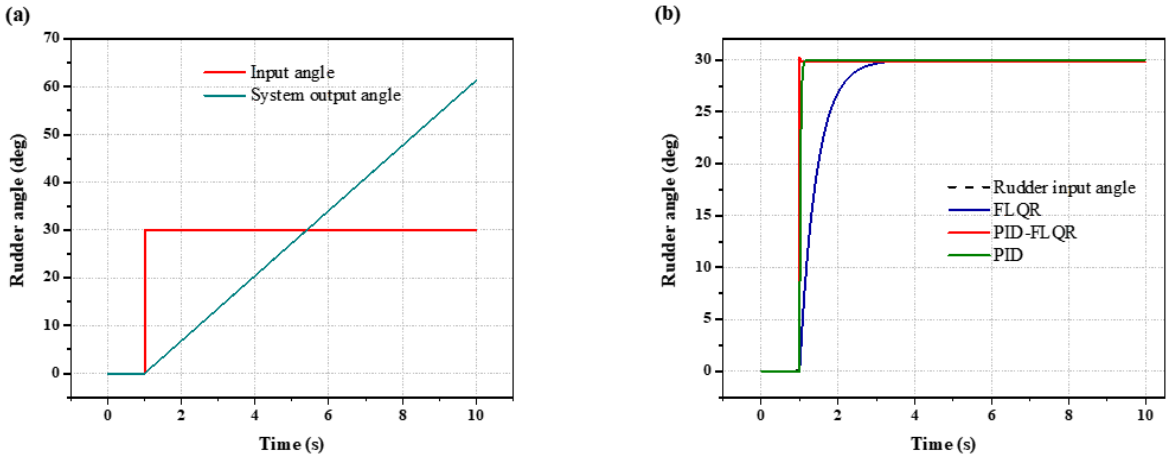

Figure 9. The time response curve of the ship's rudder angle: (a) Open-loop response, (b) Controllers' closed-loop responses.

The response curves of the system under controllers are shown in Fig.9(b), it can be observed that the PID-FLQR controller gives the fastest. The process noise and sensors measurement noise have been added to the system in Fig.10(a) and Fig.10(b). The process noise is added for defining modeling approximations, unmodeled dynamics, parameter uncertainties and model integration errors, while the measurement noise is

added for defining malfunctions in the output sensors. As the result, the effects of the noise on the PID-FLQR controller are attenuated and its oscillation's amplitudes are the lowest as compared to other controllers. Process and measurement noises cause severe oscillations to PID and FLQR controllers' response curve, those oscillations show the non-capability of the PID and the FLQR controllers keeping the system's stability under perturbations. When an uncertain heavy load disturbance is added to the steering system in Fig.10(b), a serious fall of more than $50\,\%$ is observed on the FLQR response curve. The PID-FLQR controller proved a better load rejection aptitude than the other controllers.

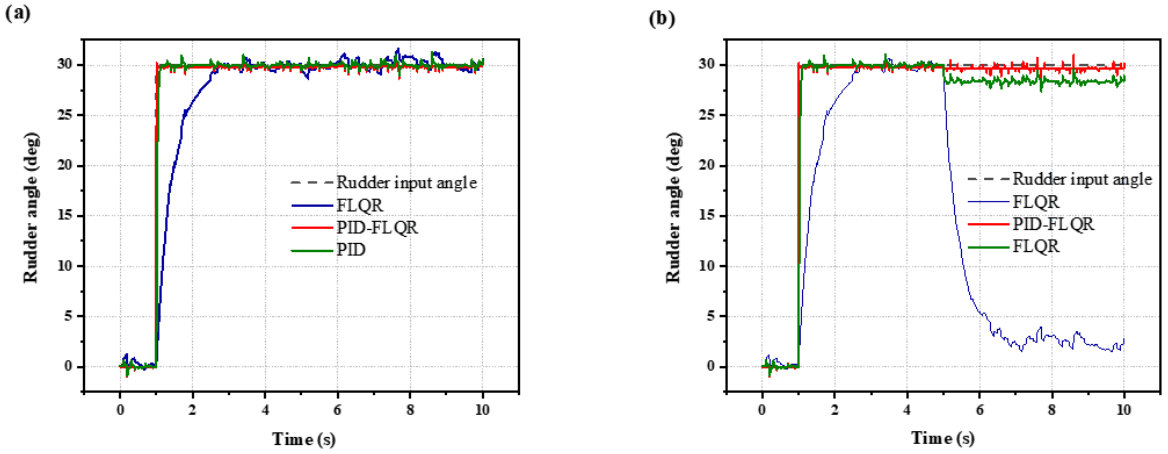

Figure 10. The time response curve of the ship's rudder angle: (a) under process and measurement noise, (b) under noise and uncertain heavy load.

The speed of the ship is reduced to $5m/s$ in Fig.11(a). Under the same conditions, changes in the PID and PID-FLQR controllers responses curves are observed, the steady-state error of the PID-FLQR controller increased, however, a serious fall is observed in the PID controller response curve. Nevertheless, the PID-FLQR still offers the best heavy load disturbance rejection capability. This result demonstrates how important ship's speed can affect the controllers' response (the responses are better when the ship's speed is high).

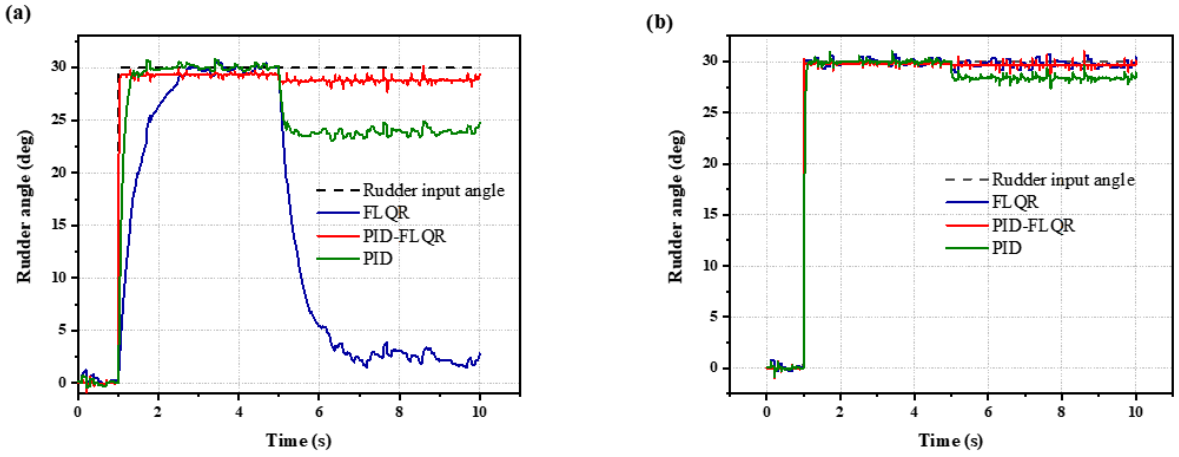

Figure 11. The time response curve of the ship's rudder angle: (a) under noise and uncertain heavy load at the speed (v=5m/s), (b) under noise and uncertain heavy load when ($Q=10^5$, $R=0.1$).

Additionally, the objective of developing a simple and cheap control system led to the choice of the weighting matrices of the FLQR controller. Thus, the performance of the controllers is made under low values of weighting matrices Q and R ($Q=10$, $R=0.1$), since it is known that when we increase the weighting matrices values, the control system is more expensive. A design decision of keeping the value of R fixed while varying the value of Q is made, simulation result in Fig.11(b) showed that the states weighting matrix Q of the FLQR controller has to be increased to $Q=10^5$ if we want the FLQR controller to reach the performance of the PID-FLQR controller in heavy load rejection.

IV. DISCUSSION

In this work, a stochastic model of a ship's electrohydraulic steering gear is developed by considering all the dynamics parameters in real navigation conditions. To control the position of the rudder, a PID-FLQR controller is designed and the simulations is run considering the sailing conditions by adding a process and a measurement noise into the system. A heavy load is also added into the system at t = 5s while running under the perturbations cited. The actual hydrodynamics forces/torques applied upon the rudder are computed in real-time using the ship's parameters such as its speed and are integrated into the controller's design for better control.

There are four major contributions in this study, firstly it has been noticed that the PID-FLQR has a faster response than the PID and FLQR controllers. Secondly, under process and measurement noise, we noticed that the oscillation amplitude in the response curves of the PID and FLQR controllers is higher compared to that of the PID-FLQR controller. The third contribution delights the robustness of the PID-FLQR controller when an uncertain heavy load applied to the system has been impeccably recovered by the PID-FLQR controller. Finally, nonetheless its simplicity the PID-FLQR controller doesn't require any high computation effort compared to the sophisticated controllers presented in the literature, its performance in load rejection is better than the classical PID controller used in ship steering control. The PID-FLQR controller requires small values weight matrices ($Q = 10,\ R = 0.1$) for good performance while the FLQR controller needs a big value of the state weight matrix ($Q = 10^5,\ R = 0.1$) for the same performance.

V. CONCLUSION

An overall mathematical model describing the ship steering drive machinery has been presented, regardless of the complexity, it has been demonstrated that the ship steering system's transfer function can be approximated by a third-order transfer function. Its open-loop response has also been shown to be non-self-balancing. A combination of classical and optimal controllers (PID-FLQR) has been proposed, implemented, and disturbed to test its response curves and compare it with the response curves of PID and FLQR controllers. The PID-FLQR exhibited good response during a heavy load rejection disturbance, and better process and measurement noises attenuation capabilities compared to the other controllers. Moreover, the proposed controller (PID-FLQR) has better performance when the ship speed is high than when the navigational speed is low. The simplicity of its design, the cheapness of its implementation, and its control performance are significant to be suggested for functional control to any kind of vessel regardless of its size and navigation target, and can also be applied to systems with large inertia, heavy load uncertainty disturbance, parameter uncertainty, and self-balance or non-self-balance systems.

REFERENCES

[1]. Liu, J., & Hekkenberg, R. (2017). Sixty years of research on ship rudders: effects of design choices on rudder performance. Ships and offshore structures, 12(4), 495-512.

[2]. Żelazny, K. (2014). Approximate method of calculating forces on rudder during ship sailing on a shipping route. TransNav: International Journal on Marine Navigation and Safety of Sea Transportation, 8(3), 459-464.

[3]. Fu, Y., Fu, J., & Liu, G. (2017, August). Fuzzy CMAC compound control of hydraulic servo actuation for ship steering system. In 2017 IEEE International Conference on Mechatronics and Automation (ICMA) (pp. 1792-1797). IEEE.

[4]. Larrazabal, J. M., & Peñas, M. S. (2016). Intelligent rudder control of an unmanned surface vessel. Expert Systems with Applications, 55, 106-117.

[5]. Yuan-bin, H. (2017). Genetic algorithm's application for optimization of PID parameters in dynamic positioning vessel. In MATEC Web of Conferences (Vol. 139, p. 00153). EDP Sciences.

[6]. Wang, L., Wu, Q., Li, S., & Liu, J. (2018). Ship course control based on bas self-optimizing PID algorithm[C]. In International Conference on Marine Simulation and Ship Maneuverability (MARSIM 2018).

[7]. Do, N. M., Nguyen, P. H., & Nguyen, D. A. (2017, July). Design and simulate a Fuzzy autopilot for an Unmanned Surface Vessel. In 2017 International Conference on System Science and Engineering (ICSSE) (pp. 454-459). IEEE.

[8]. Vo, D. D., Pham, V. A., & Nguyen, D. A. (2018, November). Design an adaptive autopilot for an unmanned surface vessel. In 2018 4th International Conference on Green Technology and Sustainable Development (GTSD) (pp. 323-328). IEEE.

[9]. Pan, C., Lai, X., Yang, S. X., & Wu, M. (2015). A bioinspired neural dynamics-based approach to tracking control of autonomous surface vehicles subject to unknown ocean currents. Neural Computing and Applications, 26(8), 1929-1938.

[10]. Zheng, H. B., & Sun, Y. S. (2011). Direct drive volume control electro-hydraulic servo system and its development situation. Machine Tool & Hydraulics, 39(2), 132-136.

[11]. Jiang, J., Su, W., & Liu, Q. (2008). Direct drive electro-hydraulic servo rotary vane steering gear. In Proceedings of the JFPS International Symposium on Fluid Power (Vol. 2008, No. 7-2, pp. 369-373). The Japan Fluid Power System Society.

[12]. Su, W. H., & Jiang, J. H. (2010). Direct drive volume control electro-hydraulic servo ship rudder. In Key Engineering Materials (Vol. 439, pp. 1388-1392). Trans Tech Publications Ltd.

[13]. Yu, Y., & Shi, B. Q. (2012). Design and Simulation of Direct Drive Volume Control Actuator. In Applied Mechanics and Materials (Vol. 155, pp. 162-166). Trans Tech Publications Ltd.

[14]. Bohan, L. (2018). Feedforward Based Linear Quadratic Optimal Tracking Control for a Class of Heavy Disturbance Systems. In 2018 Chinese Automation Congress (CAC) (pp. 1992-1996). IEEE.

[15]. Angue-Mintsa, H., Venugopal, R., Kenné, J. P., & Belleau, C. (2011). Adaptive position control of an electrohydraulic servo system with load disturbance rejection and friction compensation.

[16]. Faisandier, J., & Blot, M. (1999). Mécanismes hydrauliques et pneumatiques (p. 79). Paris, France: Dunod.

[17]. Thayer, W. J. 1965. Transfert functions for Moog servovalves, technical bulletin 103. Note technique. New York: Moog inc., 11 p.
[18]. FitzSimons, P. M., & J. J. Palazzolo. (1996). « Part I: Modeling of a One-Degree-of-Freedom Active Hydraulic Mount ». Journal of Dynamic Systems, Measurement, and Control, vol. 118, no 3, p. 439-442.
[19]. Watton, J. (1989). Fluid power systems: modeling, simulation, analog and microcomputer control. Englewood Cliffs, N.J.: Prentice-Hall, 490 p.

Yao Jianjun, "Numerical Design of Electro-Hydraulic Servo System for a Ship Rudder using PID-FLQR Controller." *International Journal of Engineering Science Invention (IJESI)*, Vol. 10(12), 2021, PP 07-17. Journal DOI- 10.35629/6734